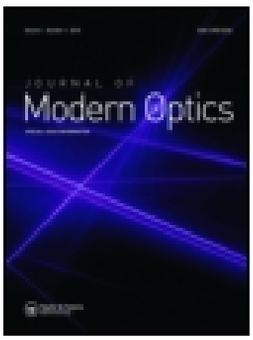

Journal of Modern Optics

ISSN: 0950-0340 (Print) 1362-3044 (Online) Journal homepage: http://www.tandfonline.com/loi/tmop20

Numerical techniques for high-throughput reflectance interference biosensing

Derin Sevenler & M. Selim Ünlü

To cite this article: Derin Sevenler & M. Selim Ünlü (2015): Numerical techniques for high-throughput reflectance interference biosensing, Journal of Modern Optics, DOI: 10.1080/09500340.2015.1117668

To link to this article: http://dx.doi.org/10.1080/09500340.2015.1117668

JOURNAL OF MODERN OPTICS, 2015
http://dx.doi.org/10.1080/09500340.2015.1117668

Taylor & Francis
Taylor & Francis Group

Numerical techniques for high-throughput reflectance interference biosensing

Derin Sevenler[a] and M. Selim Ünlü[a, b]

[a]Department of Biomedical Engineering, Boston University, Boston, MA, USA; [b]Department of Electrical & Computer Engineering, Boston University, Boston, MA, USA.

ABSTRACT

We have developed a robust and rapid computational method for processing the raw spectral data collected from thin film optical interference biosensors. We have applied this method to Interference Reflectance Imaging Sensor (IRIS) measurements and observed a 10,000 fold improvement in processing time, unlocking a variety of clinical and scientific applications. Interference biosensors have advantages over similar technologies in certain applications, for example highly multiplexed measurements of molecular kinetics. However, processing raw IRIS data into useful measurements has been prohibitively time consuming for high-throughput studies. Here we describe the implementation of a lookup table (LUT) technique that provides accurate results in far less time than naive methods. We also discuss an additional benefit that the LUT method can be used with a wider range of interference layer thickness and experimental configurations that are incompatible with methods that require fitting the spectral response.

ARTICLE HISTORY
Received 13 August 2015
Accepted 2 November 2015

KEYWORDS
Nanobiotechnology; biosensors; label free; high-throughput; interference reflectance spectroscopy; thin film interference biosensing

1. Introduction

Over the past 25 years, a variety of label-free biosensing devices have been developed around the principle of thin film reflectance interference [1–6]. Thin film interference biosensors detect the accumulation of biological film on the sensor by measuring variations in the optical thickness of thin film coated with specific molecular probes via changes in the reflectance or transmittance spectrum. Reflectometric biosensors are slightly different than 'refractometric' label free optical biosensors which often utilize surface plasmon resonance to detect biomolecular adhesion via changes in the local refractive index of the media [7,8]. Crucially, this difference may have certain advantages in situations where the refractive index of the immersion medium is not constant or precisely known: for example, quantitative detection in complex media or measurement of temperature-dependent molecular interactions [9].

Generally, reflectance interference biosensors tend to be low-cost and optically robust with limits of detection in the range of 1-10 pg mm^{-2} [2,10]. Reflectance interference biosensors can be further categorized into spectral and nonspectral (usually polarization) methods. Nonspectral methods such as Surface-enhanced Ellipsometric Contrast, Brewster Angle Straddle Interferometry, and the Adarza AIR™ image the oblique specular reflection of a narrowband light source from a near-perfect anti-reflection coating [5,6]. Biomolecule binding slightly changes the film thickness, and can be easily detected as an increase in the amount of reflected light. SEEC and AIR™ use coherent illumination, precise orientation alignment ($< 1°$), and tight tolerances on the substrate thickness to maximize sensitivity. BASI relaxes many of these tight specifications at the cost of maximum theoretical sensitivity. Since all of these techniques use oblique imaging ($50 - 70°$), they have inherent limitations on both image resolution and field-of-view.

The Interferometric Reflectance Imaging Sensor (IRIS) is a spectral approach that uses an extremely simple optical setup yet routinely obtains limits-of-detection in the range of 10-100 pg ml^{-1} [11]. IRIS utilizes a thin film reflecting $Si - SiO_2$ substrate that is imaged with a simple, large field-of-view reflecting microscope (Figure 1(*a*)). It has so far been applied in the following applications: (i) kinetics measurements of protein–protein interactions [12], (ii) kinetics measurements of DNA dehybridization for mutation detection [13], (iii) multiplexed virus screening [14], and (iv) quantification of spotting immobilization for calibrated fluorescence [15].

In IRIS, the reflectance spectrum can be sampled by sequential illumination with four narrowband LEDs and

CONTACT Derin Sevenler derin@bu.edu

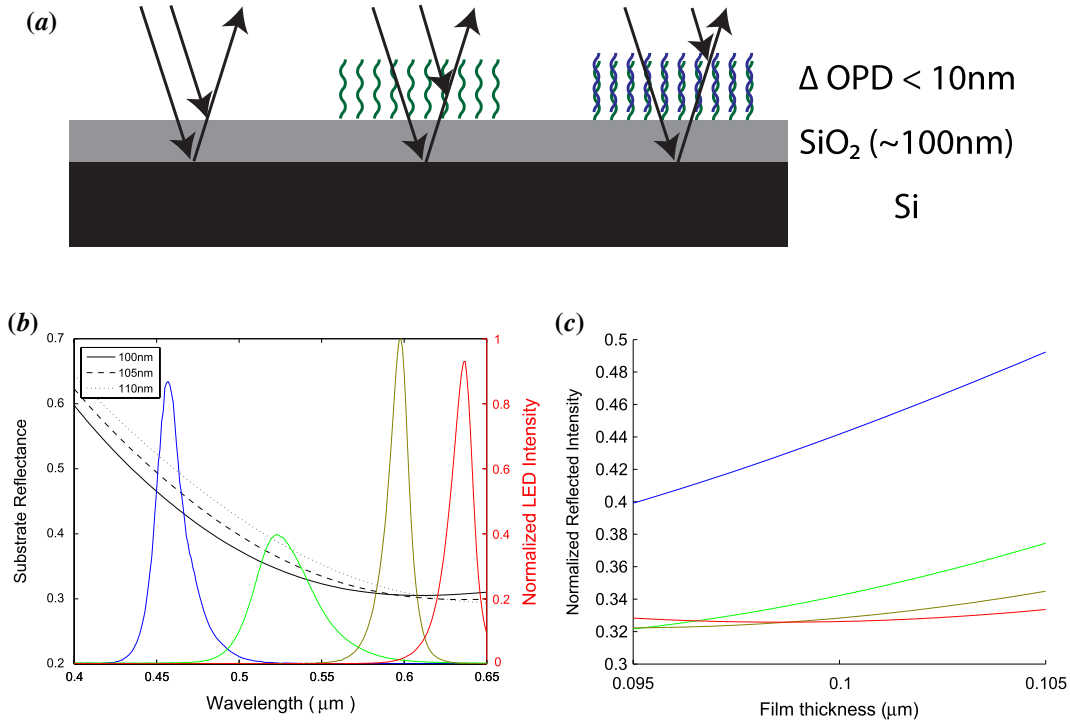

Figure 1. (*a*) Schematic of the IRIS substrate. The reflectance spectrum of a 100 nm Si – SiO_2 substrate is perturbed by the addition of biomaterial, forming the basis of multiplexed label-free biosensing with IRIS. (*b*) The reflectance spectra for 100, 105, and 110 nm IRIS substrates are superposed onto the measured illumination spectra of four LEDs used to sample the visible band. The reflectance spectra shown are modeled for normal-incidence, in air. (*c*) Normalized reflected intensities for each LED channel are shown for a range of film thicknesses. The blue channel is monotonic over this range of thicknesses and has the highest slope, so it is selected for the LUT. The reflectivity measurement is shot noise limited, so sensitivity can be greatly increased by collecting additional electrons with frame averaging. For the blue LED LUT shown here, shot noise limits sensitivity to about 500 pm for a single frame (40,000 electrons), and 50 pm for 100 averaged frames. 50 pm sensitivity corresponds with about 0.8. (The colour version of this figure is included in the online version of the journal.)

imaging onto a commercial CCD camera. Compared to higher resolution spectral measurement approaches, sampling at just four colors provides faster acquisition and greatly reduced instrument cost and complexity. The raw data is a spectral data cube, from which the filmthickness across the entire image may be calculated. This calculation is conceptually straightforward but requires significant computational power. A nonlinear least-squares curve fit must be performed for each pixel, where local film thickness is a fit parameter.

This iterative process is computationally intensive and does not scale well for high-throughput imaging-based approaches like IRIS, which can utilize large format cameras with > 10 megapixels. Whereas it may take only several seconds to analyze a single pixel on a personal computer, performing this process on even just a one megapixel data-set will take the same process over one week. Until now, there have been two approaches for processing IRIS data, both involving parallelization. The first was to submit each data-set over to a shared computing cluster with hundreds of cores. In our particular case, this approach is able to provide results within 5 to 30 min, depending on the cluster load at the time. The second approach involves using the parallel processing capabilities of a high performance graphics processing unit. This approach is able to analyze 1 MP in 5 to 10 min with current-generation GPUs.

These solutions have been adequate for demonstrating the capabilities of the IRIS approach and performing the preliminary proof-of-concept studies cited above. However, in order to unlock the potential of IRIS for high-throughput and kinetic measurement, data processing must be sped up significantly. For example, IRIS may be used to simultaneously monitor the binding kinetics of an unmodified target molecule to thousands of different species of protein, DNA or other biological molecules. However, kinetics measurements require that 10× to 100× as much raw data be collected as compared to an endpoint experiment, and monitoring thousands of spots requires imaging with 10+ MP, vs. 1 MP. With these data volumes, a current-generation GPU will take over three days to process the results of a single experiment. As the amount of collected raw data balloons, a qualitatively different approach for processing IRIS images is required.

A lookup table (LUT) is a data structure that allows the results of a computation to be saved and reused in an efficient manner. They are used widely across many different disciplines, from the multiplication tables memorized by primary schoolers to encoding Boolean logic in field-programmable gate arrays. In biosensing applications, relatively small (50 pm to 5 mm) changes in the OPD are of interest. Here we describe how implementation of a LUT side-steps these challenges of data-intensive measurements.

2. Materials and methods

2.1. Fitting the reflectance spectrum of a thin film

Here we describe the system of equations that is used to calculate film thickness from four reflected intensity measurements. In the original naive method, this is performed for every image pixel. In the new method, this is used to generate a single LUT which is rapidly applied across the entire image.

The reflectivity of a thin film is a strong function of wavelength, due to the interference of reflections at proximal and distal interfaces of the film. The extra distance travelled by waves reflecting off the distal interface is called the optical path difference (OPD) and is a function only of the index of refraction of the film and the angle of incidence. The Fresnel equations may be used to calculate the reflectance spectrum R of a simple film:

$$R = \frac{r_{12}^2 + r_{23}^2 + 2r_{12}r_{23}\cos(2\phi)}{1 + r_{12}^2 r_{23}^2 + 2r_{12}r_{23}\cos(2\phi)}; \tag{1}$$

where r_{12} represents the wavelength-dependent media–SiO_2 interface and r_{23} represents the $SiO_2 -$ Si interface:

$$r_{ab} = \frac{n_a - n_b}{n_a + n_b} \tag{2}$$

where n is the wavelength-dependent refractive index of the material. In Equation (1), ϕ is the OPD between the two reflections (again, assuming normal incidence):

$$\phi = \frac{2\pi n_2 d}{\lambda} \tag{3}$$

Here, d is the SiO_2 film thickness. The spectral reflectance curve in Equation (1) can be used to determine how much light is reflected, when illuminated with a particular source, by multiplying the source electric field amplitude $|E_{led}|$, the spectral reflectance curve R, and the camera sensor's wavelength-dependent quantum efficiency QE, and integrating over the useable bandwidth of the detector:

$$I_x(d) = \int_{\lambda=350\,\text{nm}}^{\lambda=750\,\text{nm}} \left[R(d,\lambda)\ |E_{led-x}(\lambda)|\ QE(\lambda)\right]^2 \mathrm{d}\lambda \tag{4}$$

In Equations (4) and (5) below, x is the index number of the illumination LED (i.e. 1-blue, 2-green, 3-orange, and 4-red). Combining Equation (4) for all of the LED channels provides the nonlinear system of equations that are used to solve for the film thickness.

$$\begin{bmatrix} I_{obs1} \\ I_{obs2} \\ I_{obs3} \\ I_{obs4} \end{bmatrix} = A \begin{bmatrix} I_1(d) \\ I_2(d) \\ I_3(d) \\ I_4(d) \end{bmatrix} + B \tag{5}$$

Here, A and B and film thickness d are the scalar fit parameters. This system of equations was solved with the nonlinear least-squares curve fitting solver *lsqcurvefit* in MATLAB.

2.2. Substrate and reagent preparation

$Si - SiO_2$ thin film substrates were purchased from Silicon Valley Microelectronics (Santa Clara, CA) with a nominal thickness of 100 mm and were either pre-patterned by the supplier or patterned using standard photolithography and buffered oxide etch. Substrates were diced and then coated with DMA-NAS-MAPS, a co-polymer shown to improve DNA and protein immobilization and hybridization efficiency [16]. 60-bp aminated DNA probe oligonucleotides and 62-bp unmodified target oligonucleotides with a 15-bp complementary region were purchased from Integrated DNA Technologies (Coralville, IA). DNA microarray spots of varying immobilization densities but constant size were created by varying the spotting concentration of aminated DNA from 1 to 16 μM while keeping the total DNA concentration constant by supplementing with an auxiliary nonaminated DNA species.

2.3. Measurement instrumentation and procedure

Measurements were obtained using a simple and automated optical setup described in detail elsewhere [10]. Briefly, Köhler illumination from four LEDs is projected onto the substrate via a nonpolarizing beamsplitter and imaged using a low magnification objective and a scientific camera. Sequential measurements with each LED were acquired in an automated manner using micro-manager [17]. 100 frames were acquired and averaged for each LED channel before saving to reduce shot noise.

Spatial variations in illumination were addressed by normalizing images pixel-wise with an image of clean bare silicon acquired with identical instrument settings. Temporal and inter-channel variations in illumination are addressed similarly, by normalizing each image by the average intensity within a region of bare silicon that was etched for this purpose into each IRIS substrate.

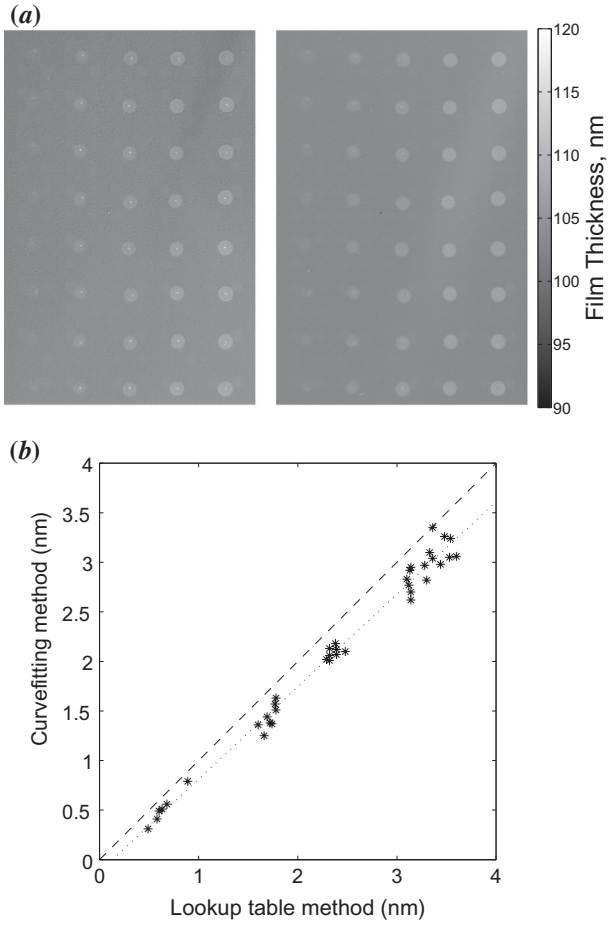

Figure 2. (*a*) Grayscale representations of the measured film thickness of a 100 nm IRIS DNA microarray, processed with either curve fitting (left) or LUT (right). A single data-set was processed using both pixel-by-pixel curve fitting on a computing cluster (MGrid approx. 8 min) and the LUT approximation on a laptop computer (approx. 50 ms). The region shown is 1.9 × 1.4 mm. (*b*) Scatterplot comparing spot heights as measured using the two techniques. The dashed line represents equivalence ($y = x$), and the dotted line represents the least-squares linear regression ($y = 0.93x - .12$, $R^2 = .91$).

2.4. LUT generation and use

The first step of processing is to normalize (divide) each image by the reflectivity of a region of bare silicon, to account for variations in illumination intensity. An etched region is identified automatically using feature recognition. The reflectivity of the SiO_2 film is then measured by automatically selecting a region of the image with no biomolecules and averaging the signal from each channel – these are I_{obs1-4} in Equation (5). Nonlinear curvefitting is used to find the parameters A, B and d – the baseline film thickness. Those parameters are then used in Equation (5) calculate the predicted reflectivity of each channel over a range of nearby film thicknesses (i.e. $d \pm 5$ nm). This is the LUT shown in Figure 1(*c*). Depending on the number of points to calculate, this step takes 10 to 30 s. Finally, this LUT is used to measure heights relative to the average baseline thickness across the rest of the image(s). In the LUT approach, not all four color channels are used once the baseline thickness is found – rather, the channel most sensitive to film thickness is selected (i.e. the channel with the greatest absolute average slope that is monotonic).

Once a LUT has been generated for a particular experimental configuration, it can be used for all subsequent experiments that use that same configuration. Since the LUT is not a linearization, it may be generated to have a wide-enough range to encapsulate manufacturing variability in film thickness (i.e. ±15 nm). A new LUT must be generated if (a) the substrate has an unknown thickness, (b) the substrate is outside the range of existing tables, or (c) some part of the optical configuration has been changed, such as the microscope objective or the immersion medium.

3. Results and discussion

To validate the LUT approach in a practical setting, an IRIS DNA microarray was imaged and processed using both curve fitting and the LUT, and compared (Figure 2(*a*)). Spot 'heights' were then calculated. The height of a microarray spot is defined as the quantitative increase in OPD caused by the immobilized DNA, as compared to the local baseline oxide thickness. Spot heights were calculated by manually selecting the boundary of each spot to find the region's average thickness, and then subtracting from that the average film thickness of a surrounding annular region. Spot height measurements were found to agree closely, but not perfectly (Figure 2). While the grayscale representations of film thickness look nearly identical, the LUT approach consistently over-estimates spot heights (as compared to curve fitting) by about 7–10%.

This systematic error between methods was not observed when comparing measurements of bare SiO_2 films of a variety of thicknesses, which suggests that its cause is linked to biological material optical properties. Indeed, both the curve fitting and LUT methods assume that the optical properties of the biological film are identical to that of the baseline film of SiO_2, to avoid more complex multi-film calculations where the optical properties of the packed biomolecules is unclear. Undoubtedly, this approximation effects the two methods differently as they each weigh the spectral information differently. However, the two methods are highly proportional ($R^2 = 0.91$), indicating that the LUT may be used as an alternative to pixel-by-pixel curve fitting. Crucially, while the curve fitting approach took about 8 min to process this data-set on a computing cluster, applying the LUT took only 50 ms once the LUT was generated. Also, the generated LUT may be

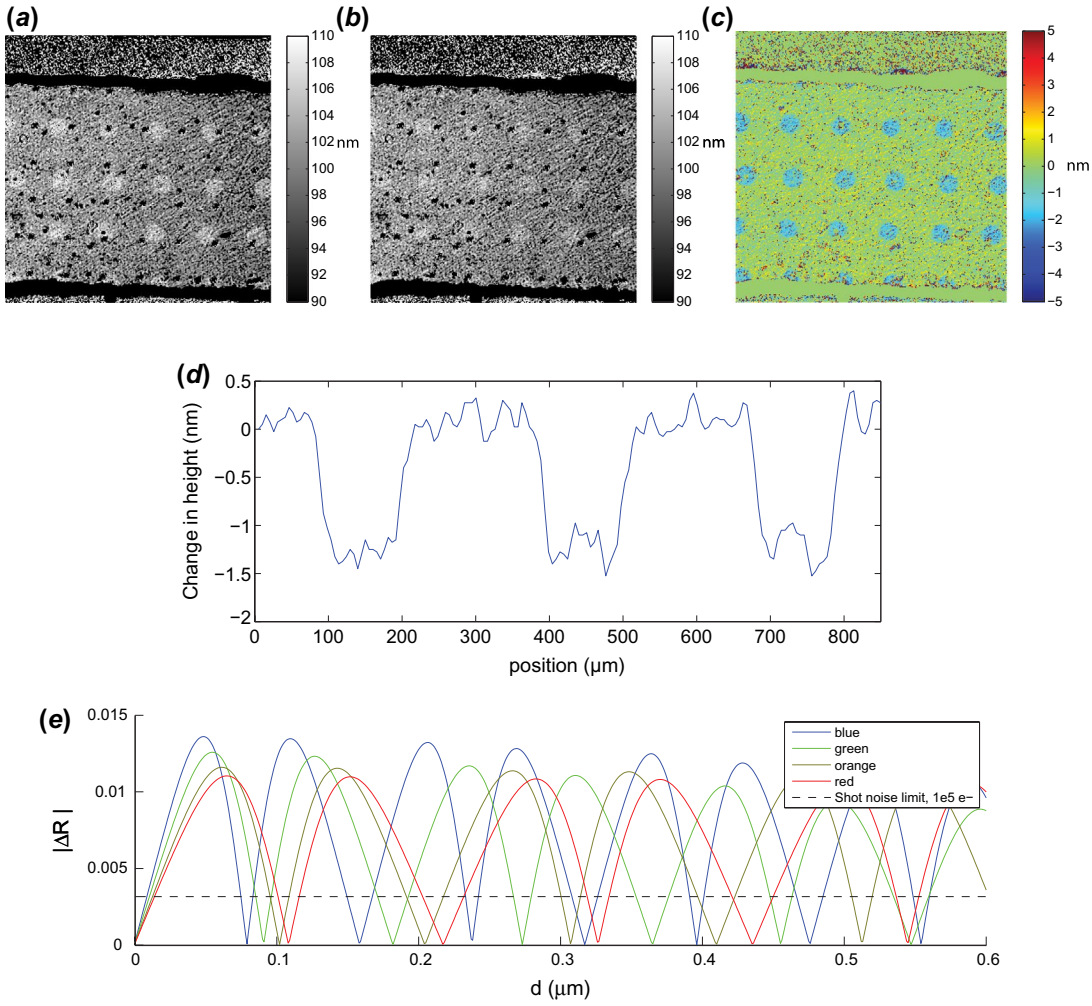

Figure 3. LUT processing can be used with substrates or configurations that cannot be measured using curve fitting. (*a*–*d*) Grayscale representations of film thickness (nanometers) calculated from IRIS measurements using a LUT, before (*a*) and after (*b*) dehybridization of unmodified DNA by flowing 0.1 M NaOH for 1 min. The residual (*c*) and 10-pixel-wide line average (*d*) show spot heights decrease by about 1.5 nm. The substrate was measured in water immediately before and after dehybridization. Processing this measurement with spectral curve fitting is impossible because the reflectance spectrum of 100 nm IRIS substrates in water monotonically decreases in the visible band. However, the LUT method can still be used to make accurate measurements. 100 frames (approx. 300,000 electrons per pixel totally) were collected and averaged for each image, taking about 10 s each – the LUT conversion from reflectance to nanometers can be performed in real time (approx. 50 ms). (*e*) Model predictions of the absolute value of the change in reflected intensity of each LED band in response to a small 1 nm step change are plotted as a function of film thickness. For a given baseline film thickness, some LED bands will be more sensitive to small changes in thickness than others. This plot shows which of the four included LED bands will be most sensitive to a small change in thickness, and therefore is the best to use for a LUT. The shot noise limit corresponding with the collection of 100,000 electrons (photons) is also shown as a reference. This plot was generated for normal incidence on an IRIS subatrate in air. (The colour version of this figure is included in the online version of the journal.)

used for analyzing all other data-sets collected with the same microscope of similar-thickness substrates.

However, in addition to its speed, LUT processing has the additional benefit of being compatible with substrates or configurations that cannot be measured with curve fitting. For example, the spectral response of a 100 nm film when immersed in water is almost a linear monotonic function of wavelength in the visible band. Therefore, the extra scaling and offset parameters A and B used in Equation (5) make it impossible to fit with sufficient accuracy. However, since the baseline oxide thickness is usually accurately measured either during fabrication or with IRIS prior to the experiment, this knowledge can be used to generate a LUT for these situations.

We demonstrated this by measuring the dehybridization of DNA from microarray spots on a 100 nm IRIS substrate in liquid (Figure 3). A DNA microarray of identical spots was incubated with its complement sequence and was then incorporated into a simple flow cell with a coverglass window and imaged while immersed 2× SSC hybridization buffer. The DNA was rapidly and thoroughly dehybridized by rinsing with 0.1 M NaOH for 1 min, then

washed with SSC and imaged again. Decreased spot height after dehybridization was clearly observed.

The LUT approach may be used with IRIS substrates over a large range of oxide thicknesses without greatly decreased accuracy. Since this approach only uses the most sensitive LED channel for the given immersion media and film thickness, an illumination source can be found to maximize sensitivity (Figure 3(*e*)). Indeed, one of the four LEDs included in the existing configuration does acceptably at any chosen thickness (i.e. 30 nm to 1 μm).

4. Conclusions

We have shown that the use of a LUT approximation may be used to process IRIS data 10,000 fold faster yet with similar sensitivity, unlocking a variety of scientific and clinical applications in biomolecular screening that require high-throughput measurement of molecular kinetics. The numerical technique discussed here is applicable to other interference-based biosensors, and the broader family of label-free optical biosensing with spectral measurement.

Acknowledgements

We are grateful to David Freedman for helpful discussions and suggestions leading up to and during this work. This work was funded by the Boston University Cross-Disciplinary Training Program in Nanotechnology and Cancer, a program of the NCI Alliance for Nanotechnology in Cancer.

Disclosure statement

No potential conflict of interest was reported by the authors.

References

[1] Kraus, G.; Brecht, A.; Vasic, V.; Gauglitz, G. *Fresenius' J. Anal. Chem.* 1994, *348*, 598–601. Doi: 10.1007/BF00323940.

[2] Brecht, A.; Gauglitz, G. *Fresenius' J. Anal. Chem.* 1994, *349*, 360–366. Doi: 10.1007/BF00326600.

[3] Lin, V.S.-Y.; Motesharei, K.; Dancil, K.-P.S.; Sailor, M.J.; Ghadiri, M.R. *Science* 1997, *278*, 840–843. Doi: 10.1126/science.278.5339.840.

[4] Carter, J.A.; Mehta, S.D.; Mungillo, M.V.; Striemer, C.C.; Miller, B.L. *Biosens. Bioelectron.* 2011, *26*, 3944–3948. Doi: 10.1016/j.bios.2011.02.025.

[5] Ausserr, D.; Valignat, M.-P. *Opt. Express* 2007, *15*, 8329–8339. Doi: 10.1364/OE.15.008329.

[6] Gao, T.; Rothberg, L.J. *Anal. Chem.* 2007, *79*, 7589–7595. Doi: 10.1021/ac071082d.

[7] Fan, X.; White, I.M.; Shopova, S.I.; Zhu, H.; Suter, J.D.; Sun, Y. *Anal. Chim. Acta* 2008, *620*, 8–26. Doi: 10.1016/j.aca.2008.05.022. http://www.sciencedirect.com/science/article/pii/S0003267008009343.

[8] Schneider, B.H.; Edwards, J.G.; Hartman, N.F. *Clin. Chem.* 1997, *43*, 1757–1763. http://www.clinchem.org/content/43/9/1757.

[9] Ewald, M.; Blanc, A.F.L.; Gauglitz, G.; Proll, G. *Anal. Bioanal. Chem.* 2013, *405*, 6461–6469. Doi: 10.1007/s00216-013-7040-9.

[10] Daaboul, G.G.; Vedula, R.S.; Ahn, S.; Lopez, C.A.; Reddington, A.R.; Özkumur, E.; Ünlü, M.S. *Biosens. Bioelectron.* 2011, *26*, 2221–2227. Doi: 10.1016/j.bios.2010.09.038. http://www.sciencedirect.com/science/article/pii/S0956566310006524.

[11] Monroe, M.R.; Daaboul, G.G.; Tuysuzoglu, A.; Lopez, C.A.; Little, F.F. M. S. nl. *Anal. Chem.* 2013, *85*, 3698–3706. Doi: 10.1021/ac4000514.

[12] Özkumur, E.; Needham, J.W.; Bergstein, D.A.; Gonzalez, R.; Cabodi, M.; Gershoni, J.M.; Goldberg, B.B.; Ünlü, M.S. *Proc. National Acad. Sci.* 2008, *105*, 7988–7992. Doi: 10.1073/pnas.0711421105. http://www.pnas.org/content/105/23/7988.

[13] Özkumur, E.; Ahn, S.; Yalçin, A.; Lopez, C.A.; Çevik, E.; Irani, R.J.; DeLisi, C.; Chiari, M.; Ünlü, M.S. *Biosens. Bioelectron.* 2010, *25*, 1789–1795. Doi: 10.1016/j.bios.2009.12.032. http://www.sciencedirect.com/science/article/pii/S0956566309007106.

[14] Lopez, C.A.; Daaboul, G.G.; Vedula, R.S.; Özkumur, E.; Bergstein, D.A.; Geisbert, T.W.; Fawcett, H.E.; Goldberg, B.B.; Connor, J.H.; Ünlü, M.S. *Biosens. Bioelectron.* 2011, *26*, 3432–3437. Doi: 10.1016/j.bios.2011.01.019. http://www.sciencedirect.com/science/article/pii/S0956566311000431.

[15] Reddington, A.P.; Monroe, M.R.; Ünlü, M.S. *Rev. Sci. Instrum.* 2013, *84*, 103702. Doi: 10.1063/1.4823790.

[16] Cretich, M.; Pirri, G.; Damin, F.; Solinas, I.; Chiari, M. *Anal. Biochem.* 2004, *332*, 67–74. Doi: 10.1016/j.ab.2004.05.041.

[17] Edelstein, A.; Amodaj, N.; Hoover, K.; Valw, R.; Stuurman, N. In Computer control of microscopes using manager. *Current Protocols in Molecular Biology*, John Wiley & Sons Inc: 2001. Doi: 10.1002/0471142727.